JGR Atmospheres

RESEARCH ARTICLE
10.1029/2019JD030262

Toward a Combined Surface Temperature Data Set for the Arctic From the Along-Track Scanning Radiometers

E. M. A. Dodd[1], K. L. Veal[1], D. J. Ghent[1], M. R. van den Broeke[2], and J. J. Remedios[1]

[1]National Centre for Earth Observation, Department of Physics and Astronomy, University of Leicester, Leicester, UK, [2]Institute for Marine and Atmospheric Research Utrecht, Utrecht University, Utrecht, Netherlands

Abstract Surface temperature data sets for, or including, the Arctic have been derived from various thermal infrared sensors. However, a combined, all surface temperature data set for the Arctic has not been generated previously. Here we present the first combined land, ocean, and ice surface temperature data set for the Arctic produced from Along-Track Scanning Radiometer - 2 and the Advanced Along-Track Scanning Radiometer satellite sensors: the Along-Track Scanning Radiometer Arctic combined Surface Temperature data set. Separate products, produced independently for each sensor and containing quantified uncertainties, together cover the period August 1995 to April 2012. Product validation, utilizing a more extensive in situ database than previous studies, shows that Along-Track Scanning Radiometer Arctic combined Surface Temperature surface temperatures generally agree with in situ data and are similar to previous validation of input surface temperature retrievals. Biases range from −1.74 to 0.23 K over open ocean, sea ice, snow over land, and the Greenland ice sheet with higher variability over snow/ice. However, there are noticeable outliers in the validation results, particularly over Arctic land in boreal summer for Along-Track Scanning Radiometer - 2, which are likely due to cloud contamination resulting from a climatologically static snow field being used for that sensor. This study suggests that the Along-Track Scanning Radiometer Arctic combined Surface Temperature data set presented here is a useful tool for assessment of models in the Arctic. Further work would have clear benefits including improvements to snow cover and cloud clearing to achieve a fully consistently processed, climate quality combined surface temperature data set for the Arctic region.

Key Points:
- This study presents the first combined surface temperature data set for the Arctic, derived here from ATSR thermal infrared satellite data
- Product validation shows data set surface temperatures generally agree with in situ data, but cloud contamination is an issue
- This combined surface temperature data set is a useful tool for assessment of models in the Arctic, although further work is required

Supporting Information:
- Supporting Information S1

Correspondence to:
E. M. A. Dodd,
emad2@le.ac.uk

Citation:
Dodd, E. M. A., Veal, K. L., Ghent, D. J., van den Broeke, M. R., & Remedios, J. J. (2019). Toward a combined surface temperature data set for the Arctic from the along-track scanning radiometers. *Journal of Geophysical Research: Atmospheres*, *124*, 6718–6736. https://doi.org/10.1029/2019JD030262

Received 4 JAN 2019
Accepted 23 MAY 2019
Accepted article online 10 JUN 2019
Published online 3 JUL 2019

©2019. The Authors.
This is an open access article under the terms of the Creative Commons Attribution-NonCommercial-NoDerivs License, which permits use and distribution in any medium, provided the original work is properly cited, the use is non-commercial and no modifications or adaptations are made.

1. Introduction

Surface temperature (ST) changes in the polar regions are predicted to be more rapid than either global averages or responses in lower latitudes. Model studies (Bracegirdle & Stephenson, 2012; Dufresne et al., 2013; Koenigk et al., 2013) consistently suggest that the polar regions have the largest climate sensitivity to greenhouse gas increases, resulting from climate amplification processes (Serreze & Barry, 2011). Observations of STs (Overland et al., 2016; Timmermans, 2016) and other changes associated with climate change (Derksen et al., 2016; Hinzman et al., 2005; Perovich et al., 2016; Tedesco et al., 2016) increasingly confirm these predictions. The impacts of this Arctic warming are not confined to this region alone; for example, they may contribute to midlatitude weather events (Cohen et al., 2014). It is, therefore, particularly important to monitor Arctic climate change.

ST changes are traditionally observed using near-surface (or 2 m) air temperatures (hereafter $T_{2\ \mathrm{m}}$) at meteorological stations. However, in situ sampling of STs is sparse both temporally and spatially. Furthermore, in the Arctic surface type varies both spatially and temporally. For example, land may be covered by permanent ice (glaciers, ice caps, and the Greenland ice sheet), seasonal snow cover, spatially varying vegetation type (mostly forest and tundra), and temporally varying fractional vegetation cover. These aspects make quantification of temperature changes over the Arctic a challenging problem but an urgent one requiring progress (Cowtan & Way, 2014; Dodd et al., 2015; Karl et al., 2015).

The polar regions are well covered by polar orbiting satellite instruments, which can provide estimates of ST at the "skin" of the Earth's surface (hereafter T_s). Satellite sensor measurements in the Thermal InfraRed (TIR) can be used to derive consistent, continuous, and detailed observations of T_s (Merchant et al., 2014). Although clouds limit TIR satellite observations of the surface to clear-sky conditions with an associated

requirement for cloud detection, microwave observations are of lower spatial resolution and very sensitive to emissivity as well as other surface parameters (Mätzler, 1994; Prigent et al., 2006; Yan et al., 2008) while in situ observations are much more sparse. Furthermore, same series TIR sensor records are also now reaching sufficient lengths to record decadal variations with good spatial coverage (Veal et al., 2013). T_s data sets for, or which include, the Arctic have been produced for ocean (Kilpatrick et al., 2015; Merchant et al., 2014; Petrenko et al., 2014), land (Ghent et al., 2017; Wan, 2014), and ice (Hall et al., 2004). The only combined analyses of Arctic surface temperature currently available are those derived from the advanced very high resolution radiometer (AVHRR); Comiso & Hall, 2014; Dybkjær et al., 2012), and indeed, the second of these (the Metop AVHRR Arctic Surface Temperature product known as MAST) is for ocean and sea ice T_s only. This paper reports a publically available all surface (land, ocean, and ice) T_s data set for the Arctic which is the first to be produced for the Along Track Scanning Radiometers (ATSRs). It will benefit regional temperature evaluations by allowing data set intercomparisons, which are important for assessing spatial disagreements between T_s data sets (Guillevic et al., 2014), and model evaluations alongside Moderate Resolution Imaging Spectroradiometer (MODIS) ice temperatures and AVHRR sea ice temperatures, as well as for future T_s observations from the Sea and Land Surface Temperature Radiometer (SLSTR) and Visible Infrared Imaging Radiometer Suite instruments. This is not only useful but could be argued to be a necessity for polar studies. There is an urgent need for satellite-based T_s data sets to document, make available, and improve Arctic temperature records for assessing models, providing model boundary conditions, and investigating temperatures across surface type boundaries (such as the marginal ice zone), for climate monitoring, climate change detection, and attribution studies.

The ATSRs were a series of TIR satellite radiometers designed explicitly for climate standard observations with a consistent approach from sensor to sensor (Veal et al., 2013). They are notable for their remarkable stability in local crossing times and calibration, high accuracy, and dual-view design which allows for more accurate atmospheric correction (Llewellyn-Jones & Remedios, 2012; Veal et al., 2013). However, it should be noted that the ATSR sensors have a narrower swath (around 500 km) compared to sensors such as MODIS (around 2,030 km) which can limit data coverage. Furthermore, there is a data gap between the loss of contact with the Advanced Along-Track Scanning Radiometer (AATSR) sensor on Envisat in 2012 and the launch of the SLSTR sensor on Sentinel 3A in 2016, which is a continuation of the ATSR series. Yet the ATSRs are well qualified to provide an accurate satellite derived data set of Arctic T_s over ocean, land, and ice. A summary of instrument details for the ATSRs is provided in Table S1 in the supporting information. Of the three ATSRs, ATSR-2 and AATSR are the most suitable; ATSR-1 data will be analyzed in due course but has additional challenges associated with it because of stratospheric aerosol contamination of radiances for ATSR-1 and some degradation in channel availability and quality. There are challenges for all sensors when producing such a combined data set over a number of years. At some point in a time series, observations require harmonization to understand differences between sensors, even those of the same sensor series, primarily due to calibration differences. Different input products to the combined data set may have inconsistencies in their land, sea, and ice masking as well as differences in their retrieval and cloud masking algorithms. Also, validation is required across different surface types and ideally should include pixels which contain a mixture of surface types.

In this work we describe the methodology, construction, and evaluation of the first combined land, ocean, and ice T_s data set for the Arctic from ATSR-2 and AATSR: the ATSR Arctic combined Surface Temperature (AAST) data set v2.1. We provide results from validation of the AAST product across different surface types, excluding mixed pixels. We define the Arctic as the area at, or north of, 60°N which encompasses the Arctic Circle and the Greenland ice sheet as well as many other definitions of the boundary of the Arctic (Przybylak, 2003). The method of surface type identification and cloud clearing, the input T_s retrievals used for each surface type, and the production of gridded mean T_s and their uncertainties are described in section 2. Results from validation of AAST data sets are described in section 3. A discussion and conclusions are provided in sections 4 and 5, respectively.

2. Materials and Methods

In producing the AAST data set our aim is to use the most accurate, physically based retrieval algorithms available. To this end, we divide the Arctic surface into four surface types and choose the most suitable T_s

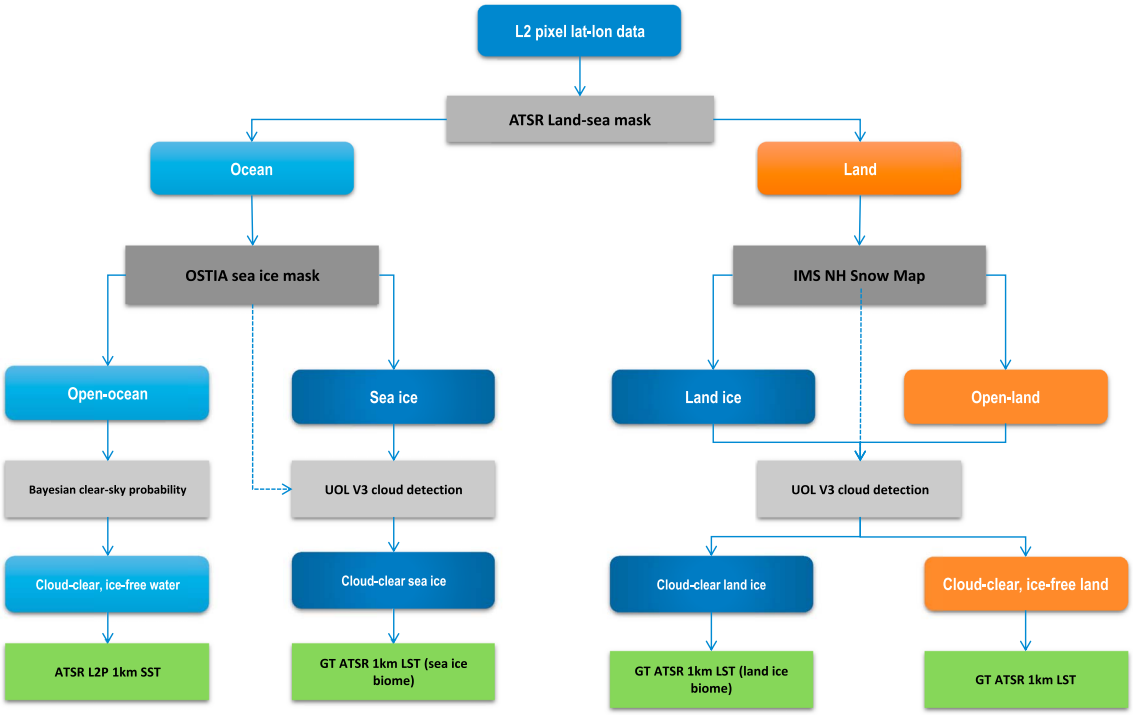

Figure 1. The masking algorithm employed in the production of the ATSR Arctic combined Surface Temperature (AAST) data set. The masking algorithm first determines surface type, thereby allowing selection of the best T_s retrieval type, and second detects the presence of cloud.

input for each. The four surface types defined are open land (land free of snow or ice), open ocean (ocean free of sea ice), land ice (land with snow or ice cover), and sea ice (sea ice with or without snow cover).

We use a masking algorithm (illustrated in Figure 1 and described in section 2.1) to determine surface type and detect cloud at each input Level 2 ATSR pixel. Level 2 (L2) data refers to geophysical variables which are derived from radiometrically calibrated and geometrically corrected radiances or brightness temperatures and provided on the orbit swath at native spatiotemporal resolution. Different L2 T_s retrieval algorithms (outlined in section 2.2) are employed for each surface type based on the masking algorithm. The AAST processor is described in section 2.3 and the output AAST Level 3 products are described in section 2.4. Level 3 (L3) data are L2 data provided at nonnative spatiotemporal resolution in a gridded map projection format. The AAST product is provided as a Level 3 Super collated (L3S) product, which is L3 data produced from L2 data from multiple instruments or sensor data sets.

2.1. Surface Type Identification and Cloud Detection

2.1.1. Land Sea Mask

The first step in determining surface type is to establish whether the pixel is land or ocean. For AAST we use the land sea mask from the standard European Space Agency (ESA) ATSR Level 1b product. The same land sea mask is used for sea surface temperature (SST) retrieval in the ATSR Sea Surface Temperature 1-km L2P v3.0 product (European Space Agency, 2014a, 2014b; hereafter SST L2P), which provides input T_s over open ocean for AAST (section 2.2.2). The GlobTemperature (GT) Land Surface Temperature (LST) 1-km L2 v2.1 product (hereafter GT LST), used for T_s over open land, land ice, and sea ice (section 2.2.1), employs a variant of the 2006 GlobCover product (Arino et al., 2007; Ghent et al., 2017) as its land sea mask to determine where to retrieve LSTs. This means that a few T_s values may be missing in AAST products due to inconsistencies between the land sea information utilized for AAST and GT LST. Pixels where T_s is provided from both input ST products will be an average of the LST and SST data available.

2.1.2. Ice Detection

After a pixel is identified as land or ocean, we determine whether a pixel is ice covered (snow or ice covered) or ice free (snow or ice free). The most difficult aspect of this is distinguishing between surface ice and cloud; clouds can have temperatures close to those of the ice surface below. In addition, the AAST product requires

a masking algorithm that will work on both nighttime and daytime data. This is due to the high-latitude phenomenon of polar day and polar night when the Sun is above, or below, the horizon for more than 24 hr and correspondingly nighttime, or daytime, data are not available. As a result of these factors, for ice and snow detection in AAST we utilize the surface classification information included in GT LST v2.1 which is provided by auxiliary data.

Permanent snow and ice extent over land is provided by a variant of the 2006 GlobCover product (Arino et al., 2007; Ghent et al., 2017). Seasonal snow and ice information in the Arctic is provided by 4-km Interactive Multisensor Snow and Ice Mapping System Northern Hemisphere (IMS) snow maps (available from 2004 onward) for land pixels (Ramsay, 1998) and the Operational Sea Surface Temperature and Sea Ice Analysis (OSTIA) over ocean pixels (Donlon et al., 2012). Preprocessing of these data sets is as described in Ghent et al. (2017). The decision was made to use 4-km IMS data because visual inspection showed it to be a much improved representation compared with the 24-km product. When IMS 4-km data are not available (prior to start of data set production) a daily climatology across all years of IMS 4-km data are used for snow detection. A climatology was used instead of lower resolution data to minimize potential step changes from moving between resolutions. In earlier years when the climatology is employed, we expect locally correlated uncertainties to be increased by 1.5 K on average in regions where snow cover may disappear based on assessments of the effects of changing the surface type of the retrieval.

Determination of the presence of ice can be done relatively successfully for daytime ATSR data using a combination of reflectance and brightness temperature thresholds, ratios, and normalized difference indices (Bulgin et al., 2015; Istomina et al., 2010). However, this task is more difficult at night when only thermal data are available from ATSR resulting in increased false flagging of cloud as ice. This is the justification for employing auxiliary ice extent data from the spatially complete daily analyses provided by OSTIA and IMS.

It should be noted that the sea ice masking information utilized in SST L2P is not the same as that employed in AAST. SST L2P sea ice information is provided by European Centre for Medium-Range Weather Forecasts Interim Reanalysis data with an additional test based on the Normalized Difference Snow Index during daytime. Therefore, some T_s data may be missing in AAST products due to differences in sea ice extent information between AAST and SST L2P.

2.1.3. Cloud Detection

The final step in the masking algorithm is the detection of cloudy pixels. AAST utilizes the cloud masking information provided in the input T_s data sets, which are produced using different algorithms. Where pixels are designated a surface type of open ocean we use the Bayesian clear-sky probability data that are part of the SST L2P (Embury et al., 2012; Mackie et al., 2010; Merchant et al., 2005). A pixel is labeled cloudy if the clear-sky probability is less than or equal to 90%. For all other pixels (surface types of open land, land ice, or sea ice) the University of Leicester version 3.0 (UOL v3) cloud masking data, provided as part of the GT LST product, are used (Ghent et al., 2017). UOL v3 is a restricted Bayesian infrared cloud detection scheme which relies on simulated radiances and specifications of the emissivity of the surface determined by biome type (Bulgin et al., 2014).

2.2. Input Surface Temperature Products

Different surface types have different emissivities and topography, and therefore require different T_s retrieval algorithms. The open ocean has fairly uniform emissivity and level topography so a dual-view retrieval is the most accurate (Embury et al., 2012; Merchant et al., 2014). It allows for more accurate atmospheric correction especially in the presence of aerosol. Open land has a range of emissivities depending on biome (type of vegetation cover) and areal vegetation extent. Land surface topography is also spatially varying. A nadir view only retrieval with different coefficients for each surface type or biome has been identified as the most suitable for LST (Coll et al., 2006; Ghent et al., 2017).

2.2.1. Open Land, Land Ice, and Sea Ice

Where the surface type is designated as open land, land ice, or sea ice by the masking algorithm, the T_s utilized for AAST are those from the GT LST v2.1 product at 1-km resolution, which is an update to the v1.0 data set described in Ghent et al. (2017). GT LST v1.0 is available from the GlobTemperature data portal (http://data.globtemperature.info/).

The GT LST product (Ghent et al., 2017) employs the Leicester ATSR and SLSTR Processor for LAnd Surface Temperature, which utilizes a nadir-only split window algorithm employing retrieval coefficients which are dependent on surface type, fractional vegetation cover, atmospheric precipitable water, and satellite view angle. Land surface emissivity is dealt with implicitly through the radiative transfer simulations used to determine the coefficients (Ghent et al., 2017). The input land surface emissivity (including land ice and snow) for these simulations is derived from the monthly 0.05° CIMMS Baseline Fit Emissivity Database (Seemann et al., 2008) while an emissivity of 0.99 (Dybkjær et al., 2012) is assumed for sea ice in coefficient production.

The pixel-level LST uncertainties are a combination of three different components representing the uncertainty from effects whose errors have distinct correlation properties: random, locally correlated, and large-scale systematic (Ghent et al., 2017). In GT LST v1.0, sea ice was retrieved using land ice coefficients. An initial validation of T_s retrievals over sea ice suggested that separate retrieval coefficients should be defined for sea ice in order to better represent this surface type. Retrieval coefficients for the sea ice surface type are included in the GT LST v2.1 data set utilized for AAST. The coefficients are determined as described for other surface types in Ghent et al. (2017). Additionally, the locally correlated uncertainties in v1.0 are provided as separate atmospheric and surface components in v2.1 and higher-resolution IMS data are employed for snow detection as noted previously in section 2.1.2.

GT LST v1.0 T_s retrievals were validated outside the Arctic and found to have good agreement with in situ data. The mean absolute biases were 1.00 and 1.08 K for daytime and nighttime, respectively, against in situ observations from 10 stations providing high quality in situ observations (Ghent et al., 2017). The robust standard deviations (RSDs) were 1.23 and 0.54 K on average across the 10 stations. Results from validation of GT LST v2.1 T_s retrievals in the Arctic are presented in this paper.

2.2.2. Open Ocean

For pixels designated as open ocean, T_s are provided by the SST L2P at 1-km resolution (European Space Agency, 2014a, 2014b), which is available from the Centre for Environmental Data Archival and uses methods based on those from the ARC L2P data set (Merchant et al., 2012). The retrieval scheme for SST is a linear combination of two (11 and 12 μm) or three (11, 12, and 3.7 μm; nighttime only) channels in either nadir or dual-view mode. Uncertainty information is provided in this data set in a similar form to those provided in the GT LST product. SST L2P retrievals have been validated globally and the median differences for AATSR and ATSR-2 dual-view retrievals were found to be less than 0.15 K with RSDs of less than 0.35 K (Corlett, 2016).

2.3. The AAST Processor

The AAST processor uses the masking algorithm described in section 2.1 to combine L2 T_s across all Arctic surfaces into L3S T_s for AATSR and ATSR-2. Separate products are produced for each sensor as both the GT LST and SST L2P products are not harmonized between sensors. This also allows users to intercalibrate the products as they wish. Yet analysis of the overlap period between 2002 and 2003, when both AATSR and ATSR-2 were operating, suggests a median bias in the ST of only 0.3 K between AAST products. The processor can provide T_s at various temporal and spatial resolutions on various spatial grids.

2.4. AAST Level-3 Super Collated Products

AAST products comprise daily T_s and their estimated uncertainties from descending and ascending ATSR overpasses (when the satellite is moving south or north, respectively) on a 0.05° longitude by 0.05° latitude grid for the area above 60°N for AATSR and ATSR-2 separately. Due to the orbits and swath of the ATSRs, coverage is limited to below 84°N. It was decided to provide the T_s on a 0.05° grid (Dodd et al., 2018) as this grid is commonly used for L3 LST and SST products and follows user requirements for LST products (Ghent et al., 2016).

AAST products are spatial averages of 1 km descending or ascending overpass T_s from the input T_s products (see section 2.2). L2 T_s from descending and ascending overpasses are averaged, weighted by the proportion of swath pixels included in the output pixel, and gridded onto separate 0.05° grids for each orbit type. Where T_s from different surface types are present within a 0.05° pixel the output pixel will be a mixture of all available input L2 T_s. If more than one descending or ascending overpass has T_s data available during a day, the output 0.05° pixel providing the observation nearest nadir, determined using the satellite zenith angle, is

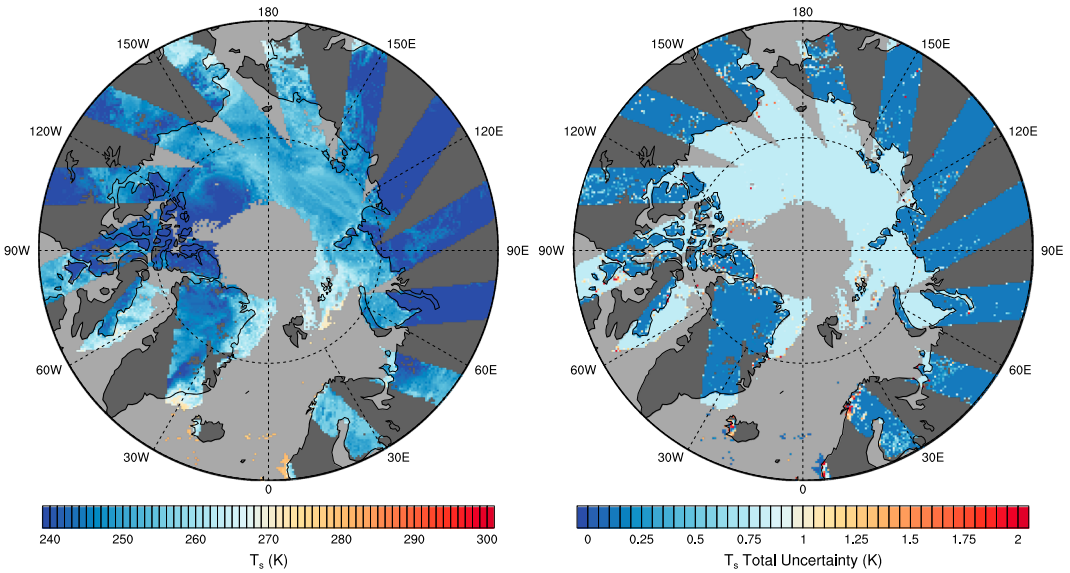

Figure 2. Example of T_S and T_S total uncertainty from the daily AAST AATSR sensor descending orbit product for 1 January 2010. This image highlights the narrow swath (around 500 km) of ATSR sensors compared to sensors such as MODIS which has a 2,030-km swath. Grey indicates areas of missing data over land (dark grey) or ocean and sea ice (light grey), either because it was not observed by the sensor or because it has been masked as cloud.

chosen. An example of T_S from the standard AAST L3S daily product is provided in Figure 2. A composite of the standard AAST L3S daily product over a month is given in Figure 3. Uncertainty information is propagated from L2 T_S to daily L3S T_S (section 2.4.1). AAST products are stored in GlobTemperature Harmonised format (Ghent et al., 2018), which provides the data in netCDF-4 format and uses CF metadata conventions.

The justification for producing ascending and descending overpass products rather than the more traditional daytime and nighttime products is twofold. First, this allows the complete seasonal cycle to be represented in both daily products for the Arctic (due to the phenomenon of polar day and night). Second, this will provide more temporally consistent view times in AAST products as (for example) the descending overpass at a given location is the same local solar time each day. The use of ascending and descending orbit products can result in different retrieval methods being combined within the same product. The LST retrieval method used for the GT LST product is the same for day and night, although different retrieval coefficients are used. The SST retrieval in SST L2P uses different channel sets for daytime and nighttime so we provide SST retrieval type as auxiliary information in AAST products.

2.4.1. Calculation and Propagation of Uncertainties

Estimates of T_S uncertainty in AAST products (0.05° grid) are propagated from the uncertainties on the input L2 surface temperature products (1-km resolution). We follow the approaches and concepts of Bulgin et al. (2016) and Ghent et al. (2017), which are equally applicable across different domains. This section provides a summary of all quantified contributory effects. Further information on the calculation and propagation of uncertainties for AAST products is given in Text S1 in the supporting information and in the cited literature.

In AAST, a four-component uncertainty model is utilized. The total uncertainty is the sum in quadrature of the random uncertainty, locally correlated atmospheric uncertainty, locally correlated biome or surface uncertainty, and large-scale systematic uncertainty. This is similar to the three-component model utilized by Ghent et al. (2017) with the locally correlated uncertainty split into two uncertainty components due to their differing correlation length scales. The four components of the uncertainty model are provided separately and also combined into a total uncertainty.

Random uncertainties, which are uncorrelated on all spatial and temporal scales, and large-scale systematic uncertainties, which are correlated on all spatial and temporal scales, are propagated using the equations of

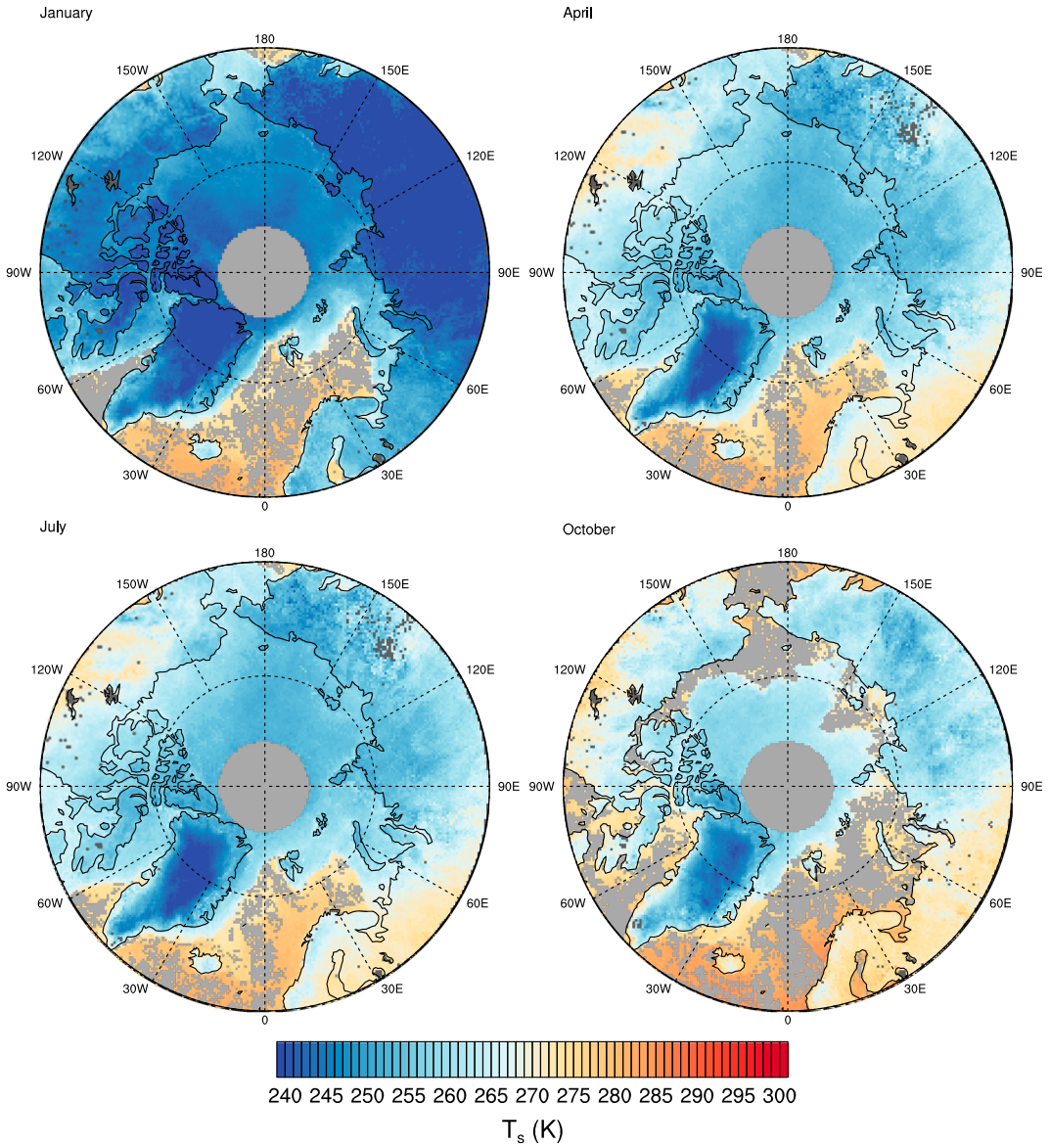

Figure 3. A composite of T_S from the daily AAST AATSR sensor descending orbit product over an example month for each season from 2010 (January, April, July, and October). Grey indicates areas of missing data over land (dark grey) or ocean and sea ice (light grey), either because it was not observed by the sensor or because it has been masked as cloud in all daily products comprising the composite.

Bulgin et al. (2016). Locally correlated atmospheric uncertainties are assumed to be correlated for the daily AAST L3S product and are propagated as such. This is because it has been recently suggested that water vapor (the main source of atmospheric uncertainty) may only be correlated on scales of a few kilometers and a few minutes (Steinke et al., 2015; Vogelmann et al., 2015), and each 0.05° pixel in AAST products is a spatial average of 1-km resolution T_s from a single swath (observed within seconds of each other). Similarly, the biome or surface correlated uncertainties are assumed to be correlated for each biome or surface type within an AAST pixel. These uncertainties are propagated as correlated uncertainties separately for each biome or surface type separately within a 0.05° pixel.

Sampling uncertainties are calculated for each 0.05° pixel, following the methods employed by the ESA GlobTemperature and EUSTACE projects (EUSTACE, 2017; GlobTemperature, 2017), using

Table 1
Summary of In Situ Sites Used for Validation in This Study. The latitude and longitude for sea ice sites are for the centre of the area through which the station drifted

Site	Surface type	Network or data source	Latitude (°N)	Longitude (°E)	Data availability in time period of interest
Tiksi	Land	BSRN	71.59	128.92	2011–2012
Barrow	Land	ARM	71.32	−156.61	1998–2012
Atqasuk	Land	ARM	70.47	−157.41	2000–2011
IMAU S5	Greenland ice sheet	UU/IMAU	67.08	−50.10	1997–2012
IMAU S6	Greenland ice sheet	UU/IMAU	67.06	−49.38	1997–2012
IMAU S9	Greenland ice sheet	UU/IMAU	67.05	−48.21	2003–2012
IMAU S10	Greenland ice sheet	UU/IMAU	67.00	−47.01	2010–2012
SHEBA	Sea Ice	ARM	77.29	−158.64	1997–1998
SEDNA	Sea Ice	SEDNA ice camp	73.28	−146.03	2007
QAANQ	Sea ice	DMI	77.5	−68.00	2011–2012
Argo floats and drifting buoys	Open ocean	Met Office Hadley Centre	Various (see Figure 4)		1995–2012

$$U^2_{sampling} = \frac{NCloud \times VarTS}{NClear + NCloud - 1} \quad (1)$$

where $\boldsymbol{U_{sampling}}$ is the sampling uncertainty, NCloud and NClear are the integer number of cloudy/clear pixels contributing to the output pixel, and VarTS is the $\boldsymbol{T_s}$ variance for clear-sky pixels contributing to the output pixel. In cases where there is no cloud and all data in a grid box are present NCloud is 0, so S is 0 and there is no sampling uncertainty.

If there are not enough clear-sky pixels to calculate VarTS, then a daily climatology value produced on a 0.05° grid is used. A few pixels do not represent enough data across a sensor record to produce a climatology variance. In these cases a daily Arctic average of the climatology variance from well-sampled pixels is assumed. Sampling uncertainties are considered part of the random uncertainty component and added in quadrature to the propagated random uncertainty to produce the total random uncertainty.

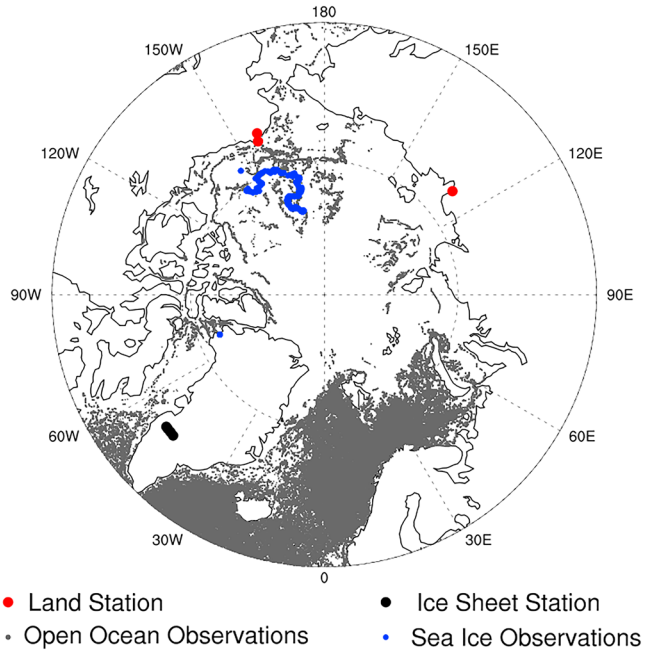

Figure 4. The location of in situ validation stations on land, the Greenland ice sheet, sea ice, and in the open ocean. In situ sea ice and open ocean observations can occur in the same location due to the spatially and temporally varying nature of sea ice cover.

3. Product Validation

The AAST products were validated against in situ T_s data derived from broadband radiometric observations over Arctic land and sea ice, and observations of SSTs at depth over open ocean areas in the Arctic. The validation method and results are described in this section.

3.1. Site Selection

Reference data for validation were obtained from sites and sensors, both drifting and stationary, situated in the areas of the Arctic observed by ATSR satellites (60°N to 84°N) during the period of interest (August 1995 to April 2012). Stationary platforms (over land and the Greenland ice sheet) were only chosen if the surrounding area was relatively homogenous in surface type and topography. A large number of measurements is required across a validation site in order to characterize it (Guillevic et al., 2012; Guillevic et al., 2014), which was not available for spatially heterogeneous sites in the area of interest. As a result, spatially homogenous sites are generally recommended for the temperature-based validation used here (Guillevic et al., 2012; Guillevic et al., 2014; Guillevic et al., 2018; Schneider et al., 2012). The in situ T_s at spatially homogenous sites are more likely to be representative of the instrument footprint, and thus, the impact of unresolved spatial and temporal representativeness on the validation is reduced. A summary of the in situ sites used for validation in this study is provided in Table 1. The locations of all reference data used are shown in Figure 4.

Several ground-based observation networks provide radiometric observations which can be used to derive in situ T_s data over land, such as the Atmospheric Radiation Measurement Climate Research Facility and the Baseline Surface Radiation Network. Three stations from these networks fulfilled the validation requirements outlined previously. In situ data over sea ice were provided by sensors deployed at several ice camps (Atmospheric Radiation Measurement, 2015; Dybkjaer et al., 2011; Hutchings, 2007). Over the Greenland ice sheet, reference data were sourced from radiometers deployed on Automatic Weather Stations by the Institute for Marine and Atmospheric Research, Utrecht University (Van de Wal et al., 2005; Van den Broeke et al., 2011). Reference data over open ocean were observations from drifting buoys and Argo floats. Quality-controlled in situ SST data from drifting buoys above 66°33′N were provided by the Met Office Hadley Centre (Corlett, 2016). Near-surface ocean temperatures from Argo floats were sourced from the Met Office Hadley Centre EN3. Only data which passed Met Office Hadley Centre quality checks and observed at depths between 3.5 and 5.5 m were used. The effects of both diurnal variability and the "cool skin" (Donlon et al., 2002) are minimized by restricting SST reference data to a regime of increased surface turbulence that is when the surface wind speed is greater than 6 m/s.

It must be noted that due to the extreme paucity of in situ T_s data in the Arctic this validation considers only a small number of locations, despite utilizing more in situ sites than previous studies. However, an investigation done during this study, which counted the land cover classification for each day of year and pixel in the Arctic, found that the in situ sites chosen represented around 60% of the surface types for an example year.

3.2. Surface Temperature Calculation and Matchup Method

In situ data from sites providing broadband radiometric observations were quality controlled and missing downwelling (atmospheric) radiation values were set to a default value of 110.3 W/m^2. T_s were then derived from these radiation data using broadband land surface emissivity data from the monthly 0.05° CIMMS Baseline Fit Emissivity Database (Seemann et al., 2008), or the ECOSTRESS spectral library for sea ice sites (Baldridge et al., 2009). Uncertainties were estimated for data from these sites by propagating the uncertainty on the radiometric observations and land surface emissivity. For sites with estimated uncertainties, only in situ data with uncertainties less than 2 K were used for this product validation. The median uncertainty is less than 0.80 K. In situ SSTs were measured at depth by Argo floats and drifting buoys.

The in situ data and satellite T_s were matched both spatially and temporally. Satellite T_s, which are equivalent to AAST data, were produced from single orbits of L2 GT LST or SST L2P data by spatially averaging across a 5 × 5 (over land and open ocean) or 11 × 11 (over sea ice) area of pixels centered on the in situ site. Satellite T_s were only validated if the standard deviation across the area was 2 K or less. Spatial averaging was performed in order to provide a Level 3 validation using data which is equivalent to an AAST L3 Uncollated product (L3 data produced from single orbits of L2 data). This increases the number of satellite data available compared to AAST L3S (daily 0.05° product providing two satellite matchups per day) allowing a better sampling of matchups for validation and a better characterization of the performance of AAST. This is especially important in a data sparse area such as the Arctic. Furthermore, due to the scale mismatch between the satellite data (5 to 11 km^2) and the in situ instruments (observing 10 m^2), in situ T_s measurements may not be representative of a single pixel satellite footprint which can observe a variety of land covers. Spatial averaging aims to also reduce the impact of unresolved spatial representativeness on the validation. We assume that the error characteristics of the in situ data and satellite T_s remain consistent. Missing data, for example, as a result of cloud masking, when combined with the paucity of in situ data here compared to other surface types, particularly reduces data availability for validation over sea ice areas. A larger spatial average was therefore employed over sea ice to further reduce the impact of missing data, in order to retain as much validation data as possible.

In order to try to further reduce the impact of unresolved spatial representativeness on the validation, only pixels which had the same surface type as expected at the site were spatially averaged to provide satellite T_s. However, it should be noted that the variability of T_s within the satellite footprint will still impact the results of this validation. The data were temporally matched to within time periods where the T_s is not expected to change notably: within 1 min over land and ice, and within 3 hr for ice free ocean following Embury et al. (2012).

Table 2
Summary of Validation Results Over Arctic Surface Types for Both ATSR Sensors of Interest in This Study Combined and Separately, As Well As Validation Results for a Standard MODIS LST Product (MOD11_L2 Collection 6) Produced Using the Same Methods for Comparison

		Median difference (K)		Robust standard deviation (K)		Number of matchups	
Surface type	Sensor(s)	Daytime	Nighttime	Daytime	Nighttime	Daytime	Nighttime
Land, snow	ATSR-2 and AATSR	−1.47	−0.80	2.46	1.93	2,536	3,043
	ATSR-2	−2.11	−0.62	3.45	2.06	669	792
	AATSR	−1.31	−0.86	2.13	1.84	1,867	2,251
Land, nonsnow	ATSR-2 and AATSR	−2.92	−2.57	4.11	3.94	723	168
	ATSR-2	−7.17	−2.33	7.98	4.74	235	34
	AATSR	−2.22	−2.57	3.23	3.75	488	134
Land (snow and nonsnow biome)	MOD11_L2 collection 6	−2.90	−1.24	2.67	2.16	4,378	5,853
Greenland ice sheet	ATSR-2 and AATSR	−0.23	−1.74	2.13	3.23	3,247	658
	ATSR-2	−0.71	−1.04	2.49	2.79	750	264
	AATSR	−0.06	−2.06	2.00	3.34	2,497	394
	MOD11_L2 collection 6	−0.54	−1.75	1.96	2.28	13,491	8,678
Sea ice	ATSR-2 and AATSR	−1.45	−0.89	2.77	1.81	108	86
	ATSR-2	−1.51	−0.82	2.71	1.87	98	80
	AATSR	−0.04	−1.65	3.05	2.16	10	6
Open ocean	ATSR-2 and AATSR	−0.19	−0.18	0.21	0.30	7,421	19,462
	ATSR-2	−0.17	−0.13	0.25	0.37	781	2,212
	AATSR	−0.19	−0.18	0.21	0.30	6640	17,250

3.3. Results

3.3.1. Ice and Land Surface Temperatures

Product validation results for ice surface temperatures and LSTs from the GT LST product were analyzed separately over snow covered land, snow-free land, the Greenland ice sheet, and sea ice. Table 2 gives a summary of the results.

Overall the product T_s showed agreement with the in situ validation data for ice- and snow-covered surfaces (Figure 5). The daytime median differences (satellite T_s − in situ T_s) for ice surface temperatures across the whole time period are −1.47, −0.23, and −1.45 K over land (ice and snow surface type), the Greenland ice sheet, and sea ice, respectively. The nighttime median differences are −0.80, −1.74, and −0.89 K, respectively. The RSDs for both illumination conditions were up to 3.23 K. These results are similar to T_s retrieval validation results for GT LST over snow- and ice-free surfaces in the midlatitudes, where median differences were between −2.41 and 2.27 K and RSDs were 1.23 and 0.54 K on average (Ghent et al., 2017). Results are generally similar between the two sensors (Table 2). For comparison, temperature-based validation results for ST products derived from MODIS are given in Table 2. A table summarizing literature results for validation of AVHRR and MODIS ST products in the Arctic is also provided in Table S2 in the supporting information (Adolph et al., 2018; Dybkjær et al., 2012; Hall et al., 2015; Key et al., 2013; Koenig & Hall, 2010; Østby et al., 2014; Wan, 2014). The results are fairly similar when comparing the AAST validation with MODIS results, with differences in performance depending on the ATSR sensor and the surface type.

The product validation results for LSTs in snow-free Arctic land areas show larger differences between in situ and satellite data than noted for ice surfaces. The median differences are −2.92 and −2.57 K for daytime and nighttime data, respectively (Table 2). The RSDs are also higher: 4.11 K for daytime data and 3.94 K for nighttime. All surface types have marked outliers in their results where satellite T_s are 10 to 20 K lower than the in situ data. These are most noticeable for Arctic land areas, both ice covered and ice free. These outliers are expected to be due to cloud contamination in the satellite data, except for two results for sea ice which we think are due to in situ data issues as the temperatures are atypical, but not implausible, for the area and time of year at which they are observed.

Additional analysis of the data over Arctic land and the Greenland ice sheet also suggested that cloud contamination is an issue. The absolute median difference (satellite T_s − in situ T_s) was found to be reduced by around 1–2 K when the percentage of clear-sky pixels (in the matchup area of 5 × 5 or 11 × 11 pixels) increased from 4 to 100%. An increase in clear-sky pixels was assumed to indicate a reduction in the likelihood of cloud contamination rather than an increase of representativeness of the satellite T_s (due to

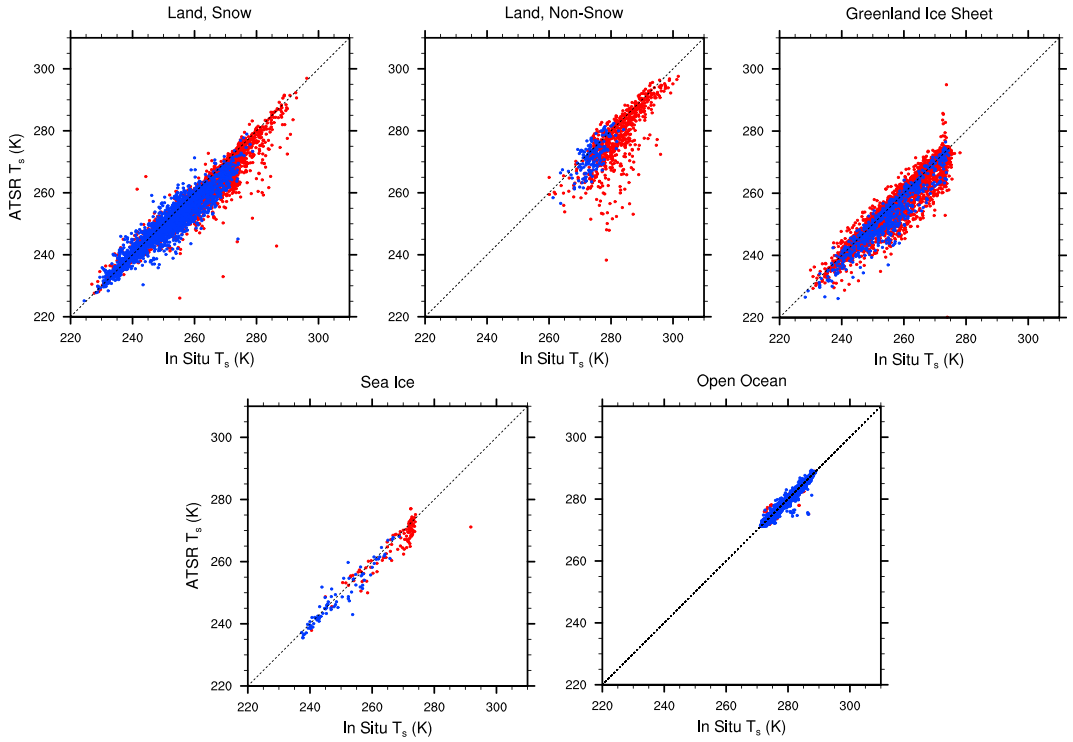

Figure 5. Scatterplots of validation results T_S from the AAST product over Arctic land, the Greenland ice sheet, Arctic sea ice, and open ocean areas above 60°N across all years of ATSR-2 and AATSR data. Daytime results are given in red and nighttime results in blue. For overall statistics from these results, see Table 2.

increased sample size of T_s in this spatial average) as the in situ sites are relatively homogenous. Absolute median differences were also found to be larger when there is a larger variance in satellite T_s across the matchup area. A large variance is assumed to indicate cloud contamination in the T_s due to a thermal contrast between the surface and clouds as the variance across the in situ site under largely clear-sky conditions is expected to be small.

To investigate these issues further the results were also investigated by month, except for sea ice due to data paucity. The monthly median differences for the Greenland ice sheet are less than 0.80 K for most months, with higher median differences (up to an absolute value of 2.60 K) in boreal winter months (Figure 6). Higher than freezing temperatures were noted in the satellite data in boreal summer, the majority of which are at the lowest elevation Institute for Marine and Atmospheric Research ice sheet site. This could be due to surface meltwater on the ice sheet or satellite pixels including areas of snow-free land surrounding the ice sheet.

Snow-covered land shows a different, and more pronounced, seasonal pattern; the monthly median differences were highest in the boreal summer and adjacent months with a maximum median difference of 4.36 K in October (Figure 7). These median differences are larger than is generally expected for ground-based LST validation in these months. Previous validation in the midlatitudes showed that GT LST data were generally within 2 K of high-quality in situ observations (Ghent et al., 2017). While snow cover in some areas persists in the Arctic throughout the year, monthly snow depth information from sources such as the NOAA National Weather Service and Zhong et al. (2018) suggest that very little or no snow cover is expected between June and September for sites providing in situ T_s data over Arctic land in this study (Barrow, Alaska; Atqasuk, Alaska; and Tiksi, Russia). Yet there is a large sample of validation results for snow T_s in June, as shown in Figure 7, and some results in July and August (up to 26 matchups) when the results are not filtered by satellite ST standard deviation. This suggests that there is erroneous classification of pixels as snow covered in GT LST over Arctic land.

The noted issues with surface misclassification of snow may result from the use of a climatology of 4-km IMS data in GT LST before this data set became available, rather than using the lower resolution 24-km product,

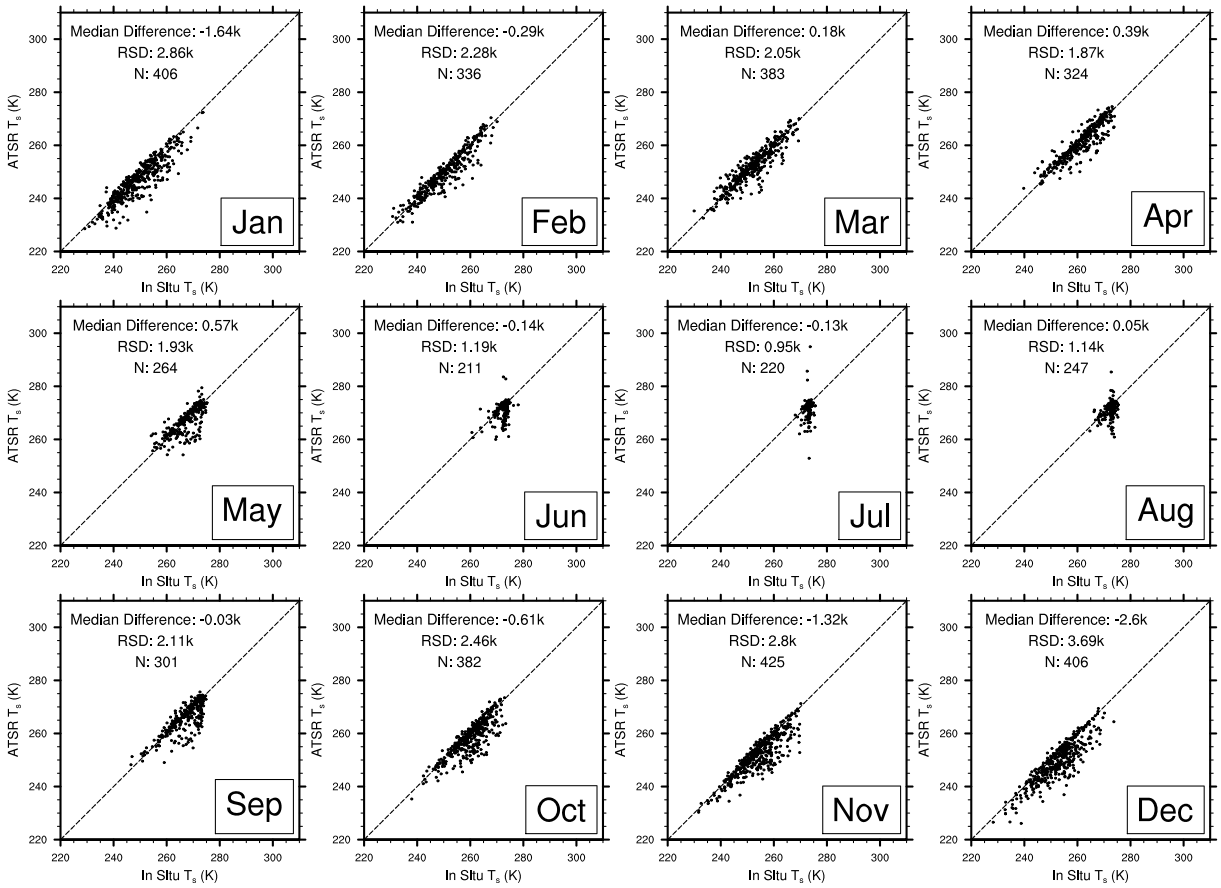

Figure 6. Scatterplots of monthly validation results for ISTs from the AAST product over the Greenland ice sheet above 60°N across all years of ATSR-2 and AATSR data. N is the number of matchups.

given the variability of snow cover extent and the rapid changes seen in recent years (Derksen et al., 2017). Median differences for before and after 2004 were compared and there was a noticeable reduction in the median differences for snow free land during the daytime, from around −4 to around −2.5 K. This can also been seen in Table 2 in the results between ATSR-2 and AATSR (the ATSR-2 record ends in 2003 and AATSR launched in 2002). Snow masking failures could also be due to errors in the IMS data set. IMS snow cover data are found to be generally comparable with other snow cover data sets and in situ data (Frei et al., 2012; Metsämäki et al., 2017). IMS provides good results for most snow types. False alarm rates are low (although relatively high compared to other data sets), except for ephemeral snow (thin and melting snow) where snow extent data sets often have poor snow detection rates (Metsämäki et al., 2017). Other studies have also noted that IMS may overestimate snow cover, particularly during snowmelt (Brown et al., 2007; Frei et al., 2012; Helfrich et al., 2007). Furthermore, snow cover can change quickly during melt and ablation and many snow cover data sets are produced at daily, or lower, temporal resolution (Nagler, 2015).

Although this version of AAST is not described as a climate quality data set, due to the need for homogenization of the sensor series among other aspects discussed in section 4, a time series analysis with respect to the Atmospheric Radiation Measurement site at Barrow was conducted for each AAST product separately. Barrow was chosen as the site is well maintained and has no obvious inhomogeneities in its record. The results are given in the supporting information.

In summary, satellite-derived T_s equivalent to AAST showed agreement with the in situ validation data but large differences were noted which are likely due to cloud contamination in GT LST, especially across Arctic land areas. Investigation of the monthly validation results suggest that this is related to surface misclassification of snow and ice, especially in boreal summer, which influences the performance of the cloud-clearing

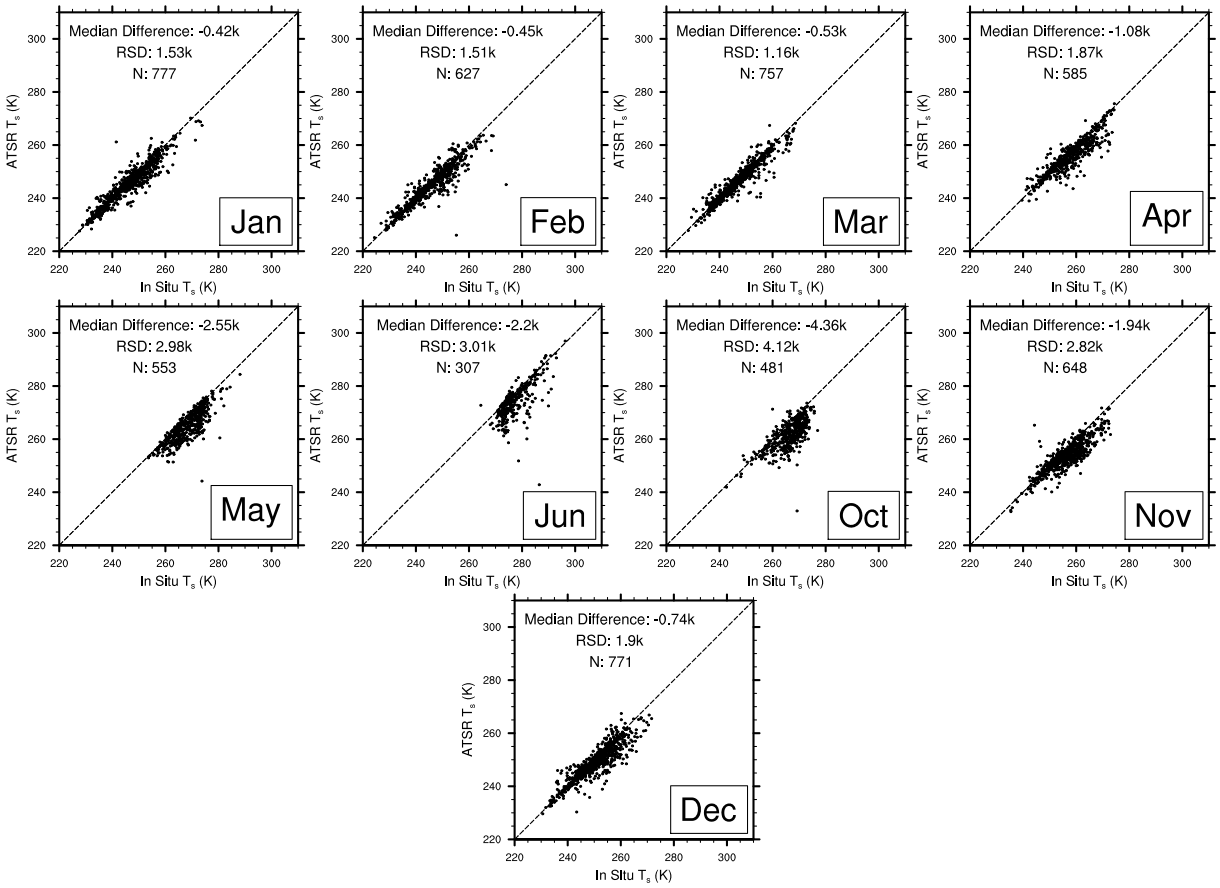

Figure 7. Scatterplots of monthly validation results for ISTs from the AAST product over Arctic land above 60°N where the surface type is ice or snow across all years of ATSR-2 and AATSR data. Only months with a reasonable sample of data in each month (more than 24 data points) are shown. N is the number of matchups.

algorithm. It should be noted that the results will also be impacted by surface misclassification under clear-sky conditions as well as the scale mismatch between the satellite and in situ data as noted in section 3.2. In addition, differences between AAST and the in situ data could also result from factors such as sensor degradation, errors in intercalibration, and errors in auxiliary data (for instance, atmospheric and emissivity data; Ghent et al., 2017). Furthermore, there could be an impact of altitude on the suitability of retrieval coefficients over land snow and ice. Most of the profiles used to generate coefficients for this surface type (which are applied globally) will be located over Greenland and Antarctica (both of which are at altitude).

3.3.2. Sea Surface Temperatures

Arctic SSTs from SST L2P agree with in situ data with a median difference of −0.19 K for daytime data and −0.18 K for nighttime data, and RSDs of 0.21 and 0.30 K for daytime and nighttime, respectively (Figure 5). These results are similar, although the differences for nighttime are slightly larger, to global validation results for SST L2P. For AATSR and ATSR-2 dual-view retrievals the median differences were less than 0.15 K and RSDs were less than 0.35 K (Corlett, 2016). Much of the bias (on the order of −0.17 K; Donlon et al., 2002) between SST L2P and in situ data will be due to comparing skin SST (AAST) with subskin (Argo floats, measured between 3.5 and 5.5 m, and drifting buoys, measured at around 20 cm) when the wind speed is more than 6 m/s (Corlett, 2016). The median differences and RSDs were very similar in all months.

4. Discussion

We have produced a first combined T_s data set for August 1995 to April 2012 for the Arctic region using ATSR data: the AAST data set. The data set combines land, sea, and ice T_s from the ATSR-2 and AATSR

instruments and includes estimated uncertainties, which are an indication of quality per pixel. There is good coverage of T_s in the daily products despite the narrow swath of the ATSR sensors.

STs equivalent to those of the AAST data set were validated across different surface types: snow-covered land, snow-free land, the Greenland ice sheet, sea ice, and open ocean. Generally, the T_s showed agreement with the in situ data and were similar to previous validation results. The daytime median differences for T_s across the whole time period were −1.47, −2.92, −0.23, −1.45, and −0.19 K over snow- and ice-covered land, snow and ice free land, the Greenland ice sheet, sea ice, and open ocean, respectively. The nighttime median differences were −0.80, −2.57, −1.74, −0.89, and −0.18 K for the different surface types, respectively. The median differences were smallest over the Greenland ice sheet and open ocean, and largest over Arctic land areas. However, there were noticeable outliers in product validation results, particularly over Arctic land areas in boreal summer months for ATSR-2, which are likely due to cloud contamination in the GT LST product.

Masking cloud cover in satellite-derived T_s data sets over land and ice is noted as being more complex than over open ocean. Over land there is cloud masking uncertainty due to land cover and land surface emissivity, which may be temporally and spatially heterogeneous between and within pixels, and elevation, which impacts view angle and atmospheric path. Cloud detection over areas covered by seasonal snow and ice is particularly difficult, especially during nighttime (Frey et al., 2008; Romano et al., 2017). Spectral responses for many wavelengths are very similar for snow and ice surfaces compared to clouds. There is also often a lack of thermal contrast between these surfaces making identification of clouds difficult. Furthermore, snow cover can change quickly during melt and ablation while ephemeral (thin or melting) snow is often difficult to detect. As a result, cloud detection uncertainties are larger for areas of snow and ice (Bulgin et al., 2018). While the UOL v3 cloud clearing algorithm is an improvement on the standard ESA ATSR cloud tests (Bulgin et al., 2014) and the use of auxiliary data to discriminate between ice-free and ice-covered surfaces works well, and avoids depending solely on TIR data for polar nighttime (extending for several months at high latitudes and when thermal contrast between snow and ice surfaces and clouds can be especially low), cloud-clearing failures are still present in the data set. This can be seen in the differences in cloud flagging between T_s data over open ocean and land in Figure 2 as well as the marked outliers noted in the product validation for all surface types.

In the product validation, outliers which were likely a result of cloud contamination in AAST were noted in the results for Arctic ice-covered and ice-free land areas. This issue was most noticeable in boreal summer, which is likely due to misclassification of seasonal snow, or other nonsnow surface types, over Arctic land. Cloud contamination is also likely to be present in other months, but may be less obvious due to a lack of thermal contrast between satellite and in situ data. Surface misclassification impacts the performance of the UOL v3 cloud-clearing algorithm as this relies on land cover information (Ghent et al., 2017). Misclassification of snow in AAST products could result from poor detection rates of ephemeral snow, the use of a climatology of 4-km IMS data prior to 2004, or the use of a daily snow cover product when snow cover can change rapidly during melt and ablation. There may also be some influence from using IMS products at a lower spatial resolution than ATSR data, which is likely to influence snow masking at snow cover margins. Other auxiliary snow extent products could be utilized for AAST in future work to improve the data set. However, results from the SnowPEx project suggest that the performance of snow extent products is similarly poor for all products investigated for ephemeral snow (Metsämäki et al., 2017). Therefore, it is likely that snow masking improvements in AAST are likely to result from improvements in IMS data rather than employing a different data set at present.

The product validation results will also have been impacted by surface misclassification under clear-sky conditions which impacts the appropriateness of the GT LST retrieval coefficients (Ghent et al., 2017). In addition, despite the methodology used, the scale mismatch between satellite and in situ data and associated T_s variability will still influence the results. Methods have been developed (Ermida et al., 2014; Guillevic et al., 2012; Guillevic et al., 2014) and continue to be developed, for example, as part of the Ground-Based Observations for Validation of Copernicus Global Land Products project (http://gbov.copernicus.acri.fr/), to upscale in situ T_s while taking account of T_s variability to make in situ T_s more comparable with satellite-derived observations. These methods could be used in the future to reduce the impact of scale mismatches when validating satellite T_s with in situ data. Additionally, these methods could enable the

validation of pixels which contain a mix of surface types, which was a challenge not addressed in this study. Furthermore, it should be noted that the results may have been impacted by factors such as sensor degradation, errors in intercalibration, errors in auxiliary data (for instance atmospheric and emissivity data), and the impacts of altitude on the suitability of retrieval coefficients applied globally over land snow and ice as the profiles used to produce these are predominately from Greenland and Antarctica.

Although an improved situation relative to previous studies, a limitation of the validation performed in this study was the narrow range of in situ sites considered due to the extreme paucity of in situ skin T_s data in the Arctic, most notably over Arctic sea ice. Only three sources of skin T_s data which were available and coincided with ATSR-2 and AATSR observations could be identified, and these were often short campaigns contributing only a few days to a month of measurements. This highlights the need for more in situ observations of T_s in the Arctic to enable validation of satellite-derived T_s products. $T_{2\ \mathrm{m}}$ could have been utilized here. This type of measurement has been used in other studies, such as Hall et al. (2004) and Dybkjær et al. (2012), to validate satellite observations as, although measured at a different height to satellite T_s, these temperatures are highly correlated (Comiso, 2003). But comparing different types of temperature is not ideal, in particular when the relationship between them can be complex (Adolph et al., 2018; Good et al., 2017; Vihma & Pirazzini, 2005). Given the sparse coverage of in situ data in the Arctic region, a detailed, spatially comprehensive intercomparison of AAST with other satellite products would likely prove useful as part of future work. This would enable investigation of the consistency of the data set with others.

As noted in section 1, there are challenges in producing a consistently processed, high-quality, combined T_s data set. Some challenges were addressed in the production of AAST, such as validating the product for different surface types, while many others remain unresolved. Different cloud clearing algorithms were utilized over land and ice compared to open ocean which is noticeable in Figure 2, where the amount of cloud masking is inconsistent across surface-type boundaries. Future work will be required to improve the cloud clearing over land and make the cloud masking more consistent across surface types. AAST products are produced separately for different ATSR sensors as the input data utilized for the current version of AAST is not harmonized. The differences between ATSR-2 and AATSR in the Arctic is around 1 K (Ghent et al., 2018). Future work should include harmonization to reduce differences between the sensors, following studies such as Good et al. (2017), Merchant et al. (2012), and Merchant et al. (2014). As noted in sections 2.1.1 and 2.1.2, land sea masking and sea ice masking are different between the SST L2P and GT LST data sets providing the input T_s for AAST. This may lead to a few missing pixels at surface-type margins where the masks are not consistent. The impact of this should be investigated and, if possible, addressed to improve the AAST data set. Future versions of AAST will aim to combine ST data sets from the ESA Climate Change Initiative, which will use a common Climate Change Initiative-wide land-sea mask. Additionally, the T_s data sets used to produce AAST use different retrieval algorithms. This is not considered an issue or a limitation here as the algorithms chosen are considered the most accurate for each surface type. But the most appropriate retrieval method for lakes was not considered in this study. Lakes cover approximately 6% of the Arctic and are important for terrestrial ecosystem processes as well as biogeochemical cycles (Paltan et al., 2015). Currently, the GT LST retrieval algorithm is used for inland water bodies, but lake focused studies use techniques such as optimal estimation to retrieve lake surface water temperatures rather than employ algorithms designed primarily for other T_s types (MacCallum & Merchant, 2012; Woolway et al., 2017). The most appropriate retrieval algorithm for lake surface water temperatures should be considered for AAST in the future. Once these aspects have been addressed a more comprehensive stability assessment should be performed. Finally, the uncertainties in AAST have not been validated and this should be addressed in the future.

5. Conclusions

The first combined T_s data set for the Arctic region has been derived from ATSR data: the AAST data set. This data set combines land, sea, and ice T_s, for separate ATSR-2 and AATSR products, and includes estimated T_s uncertainties which are an indication of quality per pixel.

Production of this data set has emphasized the challenges involved in producing a combined surface temperature data set. But given the limitations and challenges of producing a data set of this type, the overall good agreement between AAST and in situ data sets is encouraging. AAST T_s were validated against in

situ T_s data over snow-covered land, snow-free land, the Greenland ice sheet, sea ice, and open ocean in the Arctic. Generally, the satellite-derived T_s showed agreement with the in situ data and were similar to previous validation results. Biases range from −1.74 to 0.23 K for most surface types considered here, with higher variability over snow/ice. An initial time series analysis suggests that the single-sensor product records are relatively stable over time. However, there were noticeable outliers in the GT LST validation results, particularly over Arctic land areas for ATSR-2, which is likely due to cloud contamination resulting from a climatologically static snow field used for that sensor.

Modeling studies have shown that both the Arctic and the Antarctic are more sensitive than other regions to changes in the climate system. However, in situ data at high latitudes is sparse making satellite coverage of vital importance for monitoring these regions. Arctic satellite observation data sets are urgently needed for climate monitoring, for the evaluation of climate model Arctic simulations and for climate change detection and attribution studies. The work produced here suggests that ATSR Arctic Surface Temperature data set is a useful tool for assessment of models. The current version represents a good quality, long-term ATSR data set for the Arctic. While it has much value, it is not a fully rigorous climate data set. Users for climate-related applications should take careful note of the uncertainties in the data, the validation results shown here and in particular the lack of sensor homogenization.

Further work to improve this data set would ideally include efforts to address the challenges and issues noted, such as improving cloud masking in the Arctic. This data set could also be extended back into the ATSR1 period and forward to the SLSTR period, with appropriate and robust gap bridging and filling. Gap bridging and filling is required due to a data gap between the loss of contact with the AATSR sensor on Envisat in 2012 and the launch of SLSTR on Sentinel 3A in 2016. Achieving these improvements and extensions to the AAST data set would provide a continuous, consistently processed, high-quality, independent record of combined T_s in the Arctic from 1991 to present, coinciding with a time period in which large changes are known to have occurred in this region.

Acknowledgments
The research presented in this paper was funded by The UK Department for Business, Energy, and Industrial Strategy (formally The UK Department of Energy and Climate Change). Darren Ghent is funded by the European Space Agency and a NERC grant to the National Centre for Earth Observation (NCEO) in the UK. This research used the ALICE High Performance Computing Facility at the University of Leicester and the CEDA JASMIN super-data-cluster. AAST data are freely available from the CEDA Archive (https://doi.org/10.5285/b8141fa5842b45e8863816da536def5a). The authors would like to thank Gary Corlett for providing access to in situ SST data used in this study.

References

Adolph, A. C., Albert, M. R., & Hall, D. K. (2018). Near-surface temperature inversion during summer at Summit, Greenland, and its relation to MODIS-derived surface temperatures. *The Cryosphere*, *12*(3), 907–920. https://doi.org/10.5194/tc-12-907-2018

Arino, O., Gross, D., Ranera, F., Leroy, M., Bicheron, P., Brockman, C., et al. (2007). GlobCover: ESA service for global land cover from MERIS, paper presented at 2007 IEEE International Geoscience and Remote Sensing Symposium, IEEE.

ARM (2015). In T. ARM (Ed.), *Sky and ground radiometers for longwave radiation. 1997–1998, 77°17′24.0″N, 158°38′24.0″W: Mobile site at SHEBA*. Oak Ridge, USA: ARM Data Archive.

Baldridge, A., Hook, S., Grove, C., & Rivera, G. (2009). The ASTER spectral library version 2.0. *Remote Sensing of Environment*, *113*(4), 711–715. https://doi.org/10.1016/j.rse.2008.11.007

Bracegirdle, T. J., & Stephenson, D. B. (2012). On the robustness of emergent constraints used in multimodel climate change projections of Arctic warming. *Journal of Climate*, *26*(2), 669–678.

Brown, R., Derksen, C., & Wang, L. (2007). Assessment of spring snow cover duration variability over northern Canada from satellite datasets. *Remote Sensing of Environment*, *111*(2-3), 367–381. https://doi.org/10.1016/j.rse.2006.09.035

Bulgin, C., Sembhi, H., Ghent, D., Remedios, J., & Merchant, C. (2014). Cloud-clearing techniques over land for land-surface temperature retrieval from the Advanced Along-Track Scanning Radiometer. *International Journal of Remote Sensing*, *35*(10), 3594–3615. https://doi.org/10.1080/01431161.2014.907941

Bulgin, C. E., Eastwood, S., Embury, O., Merchant, C. J., & Donlon, C. (2015). The sea surface temperature climate change initiative: Alternative image classification algorithms for sea-ice affected oceans. *Remote Sensing of Environment*, *162*, 396–407. https://doi.org/10.1016/j.rse.2013.11.022

Bulgin, C. E., Embury, O., Corlett, G., & Merchant, C. J. (2016). Independent uncertainty estimates for coefficient based sea surface temperature retrieval from the Along-Track Scanning Radiometer instruments. *Remote Sensing of Environment*, *178*, 213–222. https://doi.org/10.1016/j.rse.2016.02.022

Bulgin, C. E., Merchant, C. J., Ghent, D., Klüser, L., Popp, T., Poulsen, C., & Sogacheva, L. (2018). Quantifying uncertainty in satellite-retrieved land surface temperature from cloud detection errors. *Remote Sensing*, *10*(4), 616. https://doi.org/10.3390/rs10040616

Cohen, J., Screen, J. A., Furtado, J. C., Barlow, M., Whittleston, D., Coumou, D., et al. (2014). Recent Arctic amplification and extreme mid-latitude weather. *Nature Geoscience*, *7*(9), 627–637. https://doi.org/10.1038/ngeo2234

Coll, C., Caselles, V., Galve, J. M., Valor, E., Niclòs, R., & Sánchez, J. M. (2006). Evaluation of split-window and dual-angle correction methods for land surface temperature retrieval from Envisat/Advanced Along Track Scanning Radiometer (AATSR) data. *Journal of Geophysical Research*, *111*, D12105. https://doi.org/10.1029/2005JD006830

Comiso, J. C. (2003). Warming trends in the Arctic from clear sky satellite observations. *Journal of Climate*, *16*(21), 3498–3510. https://doi.org/10.1175/1520-0442(2003)016<3498:WTITAF>2.0.CO;2

Comiso, J. C., & Hall, D. K. (2014). Climate trends in the Arctic as observed from space. *Wiley Interdisciplinary Reviews: Climate Change*, *5*(3), 389–409.

Corlett, G. (2016). ATSR v3.0 sea surface temperature validation report: Technical note for the ATSR QWG*Rep*., https://atsrsensors.org/pdf/ATSR_V3_SST_Validation_Report_Issue1A.

Cowtan, K., & Way, R. G. (2014). Coverage bias in the HadCRUT4 temperature series and its impact on recent temperature trends. *Quarterly Journal of the Royal Meteorological Society*, *140*(683), 1935–1944. https://doi.org/10.1002/qj.2297

Derksen, C., Brown, R., Mudryk, L., & Luojus, K. (2016). Terrestrial snow cover *Rep*., NOAA Arctic Program.

Derksen, C., Brown, R., Mudryk, L., Luojus, K., & Helfrich, S. (2017). Terrestrial snow cover *Rep*., NOAA Arctic Program.

Dodd, E., Veal, K., & Ghent, D. (2018). Along Track Scanning Radiometers Arctic combined Surface Temperature (AAST) daily mean level 3 (L3S) dataset, v2.1, edited, Centre for Environmental Data Analysis, Centre for Environmental Data Analysis. https://doi.org/10.5285/b8141fa5842b45e8863816da536def5a

Dodd, E. M., Merchant, C. J., Rayner, N. A., & Morice, C. P. (2015). An Investigation into the impact of using various techniques to estimate Arctic surface air temperature anomalies. *Journal of Climate*, *28*(5), 1743–1763. https://doi.org/10.1175/JCLI-D-14-00250.1

Donlon, C., Minnett, P., Gentemann, C., Nightingale, T., Barton, I., Ward, B., & Murray, M. (2002). Toward improved validation of satellite sea surface skin temperature measurements for climate research. *Journal of Climate*, *15*(4), 353–369. https://doi.org/10.1175/1520-0442(2002)015<0353:TIVOSS>2.0.CO;2

Donlon, C. J., Martin, M., Stark, J., Roberts-Jones, J., Fiedler, E., & Wimmer, W. (2012). The operational sea surface temperature and sea ice analysis (OSTIA) system. *Remote Sensing of Environment*, *116*, 140–158. https://doi.org/10.1016/j.rse.2010.10.017

Dufresne, J.-L., Foujols, M.-A., Denvil, S., Caubel, A., Marti, O., Aumont, O., et al. (2013). Climate change projections using the IPSL-CM5 Earth System Model: From CMIP3 to CMIP5. *Climate Dynamics*, *40*(9-10), 2123–2165.

Dybkjaer, G., Hoyer, J. L., Tonboe, R., Olsen, S., Rodwell, S., & Wimmer, W. (2011). The Qaanaaq Sea Ice Thermal Emission EXperiment field and data report*Rep*. http://www.dmi.dk/fileadmin/Rapporter/TR/tr11-18.pdf

Dybkjær, G., Tonboe, R., & Høyer, J. (2012). Arctic surface temperatures from Metop AVHRR compared to in situ ocean and land data. *Ocean Science*, *8*(6), 959–970. https://doi.org/10.5194/os-8-959-2012

Embury, O., Merchant, C. J., & Corlett, G. K. (2012). A reprocessing for climate of sea surface temperature from the along-track scanning radiometers: Initial validation, accounting for skin and diurnal variability effects. *Remote Sensing of Environment*, *116*, 62–78. https://doi.org/10.1016/j.rse.2011.02.028

Ermida, S. L., Trigo, I. F., DaCamara, C. C., Göttsche, F. M., Olesen, F. S., & Hulley, G. (2014). Validation of remotely sensed surface temperature over an oak woodland landscape—The problem of viewing and illumination geometries. *Remote Sensing of Environment*, *148*, 16–27. https://doi.org/10.1016/j.rse.2014.03.016

European Space Agency (2014a). AATSR: L2P Product (AATSR L2P) sea surface temperature values, v2.1., edited, NERC Earth Observation Data Centre.

European Space Agency (2014b). ATSR-2: L2P Product (ATSR-2 L2P) sea surface temperature values, v2.1., edited, NERC Earth Observation Data Centre.

EUSTACE (2017). EUSTACE Project: Using surface skin temperature from satellites to estimate daily air temperature everywhere., edited, https://www.eustaceproject.eu/

Frei, A., Tedesco, M., Lee, S., Foster, J., Hall, D. K., Kelly, R., & Robinson, D. A. (2012). A review of global satellite-derived snow products. *Advances in Space Research*, *50*(8), 1007–1029. https://doi.org/10.1016/j.asr.2011.12.021

Frey, R. A., Ackerman, S. A., Liu, Y., Strabala, K. I., Zhang, H., Key, J. R., & Wang, X. (2008). Cloud detection with MODIS. Part I: Improvements in the MODIS cloud mask for collection 5. *Journal of Atmospheric and Oceanic Technology*, *25*(7), 1057–1072. https://doi.org/10.1175/2008JTECHA1052.1

Ghent, D., Corlett, G., Gottsche, F., & Remedios, J. (2017). Global land surface temperatures from the Along-Track Scanning Radiometers. *Journal of Geophysical Research: Atmospheres*, *122*, 12,167–12,193. https://doi.org/10.1002/2017JD027161

Ghent, D., Trigo, I., Gottsche, F., Sardou, O., Bulgin, C., Prigent, C., et al. (2016). Technical specification document, v2.0*Rep*.

Ghent, D., Trigo, I., Pires, A., Sardou, O., Bruniquel, J., Göttsche, F., et al. (2018). Product user guide v3.0*Rep*., http://www.globtemperature.info/index.php/public-documentation/deliverables-1/108-globtemperature-product-user-guide/file

GlobTemperature (2017). GlobTemperature Project, edited. http://www.globtemperature.info/

Good, E. J., Ghent, D. J., Bulgin, C. E., & Remedios, J. J. (2017). A spatiotemporal analysis of the relationship between near-surface air temperature and satellite land surface temperatures using 17 years of data from the ATSR series. *Journal of Geophysical Research: Atmospheres*, *122*, 9185–9210. https://doi.org/10.1002/2017JD026880

Guillevic, P., Gottsche, F., Nickeson, J., Hulley, G., Ghent, D., Yu, Y., et al. (2018). Land Surface Temperature Product Validation Best Practice Protocol. Version 1.1. In P. Guillevic, F. Gottsche, J. Nickeson, & M. Roman (Eds.), *Best Practice for Satellite Derived Land Product Validation* (p.58): Land Product Validation Subgroup (WGCV/CEOS). https://doi:10.5067/doc/ceoswgcv/lpv/lst.001

Guillevic, P. C., Biard, J. C., Hulley, G. C., Privette, J. L., Hook, S. J., Olioso, A., et al. (2014). Validation of land surface temperature products derived from the Visible Infrared Imaging Radiometer Suite (VIIRS) using ground-based and heritage satellite measurement. *Remote Sensing of Environment*, *154*(154), 19–37. https://doi.org/10.1016/j.rse.2014.08.013

Guillevic, P. C., Privette, J. L., Coudert, B., Palecki, M. A., Demarty, J., Ottlé, C., & Augustine, J. A. (2012). Land surface temperature product validation using NOAA's surface climate observation networks—Scaling methodology for the Visible Infrared Imager Radiometer Suite (VIIRS). *Remote Sensing of Environment*, *124*, 282–298. https://doi.org/10.1016/j.rse.2012.05.004

Hall, D. K., Key, J. R., Casey, K. A., Riggs, G. A., & Cavalieri, D. J. (2004). Sea ice surface temperature product from MODIS. *IEEE Transactions on Geoscience and Remote Sensing*, *42*(5), 1076–1087. https://doi.org/10.1109/tgrs.2004.825587

Hall, D. K., Nghiem, S. V., Rigor, I. G., & Miller, J. A. (2015). Uncertainties of temperature measurements on snow-covered land and sea ice from in situ and MODIS data during BROMEX. *Journal of Applied Meteorology and Climatology*, *54*(5), 966–978. https://doi.org/10.1175/JAMC-D-14-0175.1

Helfrich, S. R., McNamara, D., Ramsay, B. H., Baldwin, T., & Kasheta, T. (2007). Enhancements to, and forthcoming developments in the Interactive Multisensor Snow and Ice Mapping System (IMS). *Hydrological Processes*, *21*(12), 1576–1586. https://doi.org/10.1002/hyp.6720

Hinzman, L. D., Bettez, N. D., Bolton, W. R., Chapin, F. S., Dyurgerov, M. B., Fastie, C. L., et al. (2005). Evidence and implications of recent climate change in northern Alaska and other arctic regions. *Climatic Change*, *72*(3), 251–298. https://doi.org/10.1007/s10584-005-5352-2

Hutchings, J. K. (2007). The Sea Ice Experiment: Dynamic Nature of the Arctic (SEDNA)-Applied Physics Laboratory Ice Station (APLIS) 2007-Field Report, edited, http://psc.apl.washington.edu/sea_ice_cdr/documentation/airborne_em/SEDNAfieldReport.pdf

Istomina, L., von Hoyningen-Huene, W., Kokhanovsky, A., & Burrows, J. (2010). The detection of cloud-free snow-covered areas using AATSR measurements. *Atmospheric Measurement Techniques*, *3*(4), 1005–1017.

Karl, T. R., Arguez, A., Huang, B., Lawrimore, J. H., McMahon, J. R., Menne, M. J., et al. (2015). Possible artifacts of data biases in the recent global surface warming hiatus. *Science*, *348*(6242), 1469–1472. https://doi.org/10.1126/science.aaa5632

Key, J. R., Mahoney, R., Liu, Y., Romanov, P., Tschudi, M., Appel, I., et al. (2013). Snow and ice products from Suomi NPP VIIRS. *Journal of Geophysical Research: Atmospheres*, *118*, 12,816–812,830. https://doi.org/10.1002/2013JD020459

Kilpatrick, K., Podestá, G., Walsh, S., Williams, E., Halliwell, V., Szczodrak, M., et al. (2015). A decade of sea surface temperature from MODIS. *Remote Sensing of Environment*, *165*, 27–41. https://doi.org/10.1016/j.rse.2015.04.023

Koenig, L. S., & Hall, D. K. (2010). Comparison of satellite, thermochron and air temperatures at Summit, Greenland, during the winter of 2008/09. *Journal of Glaciology*, *56*(198), 735–741. https://doi.org/10.3189/002214310793146269

Koenigk, T., Devasthale, A., & Karlsson, K.-G. (2013). Summer sea ice albedo in the Arctic in CMIP5 models. *Atmospheric Chemistry and Physics Discussions*, *13*(9), 25,219–25,251. https://doi.org/10.5194/acpd-13-25219-2013

Llewellyn-Jones, D., & Remedios, J. (2012). The Advanced Along Track Scanning Radiometer (AATSR) and its predecessors ATSR-1 and ATSR-2: An introduction to the special issue. *Remote Sensing of Environment*, *116*, 1–3. https://doi.org/10.1016/j.rse.2011.06.002

MacCallum, S. N., & Merchant, C. J. (2012). Surface water temperature observations of large lakes by optimal estimation. *Canadian Journal of Remote Sensing*, *38*(1), 25–45. https://doi.org/10.5589/m12-010

Mackie, S., Merchant, C., Embury, O., & Francis, P. (2010). Generalized Bayesian cloud detection for satellite imagery. Part 2: Technique and validation for daytime imagery. *International Journal of Remote Sensing*, *31*(10), 2595–2621. https://doi.org/10.1080/01431160903051711

Mätzler, C. (1994). Passive microwave signatures of landscapes in winter. *Meteorology and Atmospheric Physics*, *54*(1–4), 241–260. https://doi.org/10.1007/BF01030063

Merchant, C., Harris, A., Maturi, E., & MacCallum, S. (2005). Probabilistic physically based cloud screening of satellite infrared imagery for operational sea surface temperature retrieval. *Quarterly Journal of the Royal Meteorological Society*, *131*(611), 2735–2755. https://doi.org/10.1256/qj.05.15

Merchant, C. J., Embury, O., Rayner, N. A., Berry, D. I., Corlett, G., Lean, K., et al. (2012). A twenty-year independent record of sea surface temperature for climate from Along Track Scanning Radiometers. *Journal of Geophysical Research*, *117*, C12013. https://doi.org/10.1029/2012JC008400

Merchant, C. J., Embury, O., Roberts-Jones, J., Fiedler, E., Bulgin, C. E., Corlett, G. K., et al. (2014). Sea surface temperature datasets for climate applications from phase 1 of the European Space Agency Climate Change Initiative (SST CCI). *Geoscience Data Journal*, *1*(2), 179–191. https://doi.org/10.1002/gdj3.20

Metsämäki, S., Ripper, E., Mattila, O.-P., Fernandes, R., Schwaizer, G., Luojus, K., et al. (2017). Evaluation of Northern Hemisphere and regional snow extent products within ESA SnowPEx-project, paper presented at Geoscience and Remote Sensing Symposium (IGARSS), 2017 IEEE International, IEEE.

Nagler, T. E. A. (2015). SnowPEx—The Satellite Snow Product Intercomparison and Evaluation Exercise Deliverable 3: Review of algorithms and products *Rep*., http://snowpex.enveo.at/documents.html

Østby, T. I., Schuler, T. V., & Westermann, S. (2014). Severe cloud contamination of MODIS land surface temperatures over an Arctic ice cap, Svalbard. *Remote Sensing of Environment*, *142*, 95–102.

Overland, K. J., Hanna, E., Hanssen-Bauer, I., Kim, S.-J., Walsh, J. E., Wang, M., et al. (2016). Surface air temperature*Rep*., NOAA Arctic Program.

Paltan, H., Dash, J., & Edwards, M. (2015). A refined mapping of Arctic lakes using Landsat imagery. *International Journal of Remote Sensing*, *36*(23), 5970–5982. https://doi.org/10.1080/01431161.2015.1110263

Perovich, D., Meier, W., Tschudi, M., Farrell, S., Gerland, S., Hendricks, S., et al. (2016). Sea ice *Rep*., NOAA Arctic Program.

Petrenko, B., Ignatov, A., Kihai, Y., Stroup, J., & Dash, P. (2014). Evaluation and selection of SST regression algorithms for JPSS VIIRS. *Journal of Geophysical Research: Atmospheres*, *119*, 4580–4599. https://doi.org/10.1002/2013JD020637

Prigent, C., Aires, F., & Rossow, W. B. (2006). Land surface microwave emissivities over the globe for a decade. *Bulletin of the American Meteorological Society*, *87*(11), 1573–1584. https://doi.org/10.1175/BAMS-87-11-1573

Przybylak, R. (2003). Boundaries of the Arctic. In R. Sadourny & L. A. Mysak (Eds.), *The Climate of the Arctic* (pp. 1–4). Dordrecht, The Netherlands: Kluwer Academic Publishers. https://doi.org/10.1007/978-94-017-0379-6_1

Ramsay, B. H. (1998). The interactive multisensor snow and ice mapping system. *Hydrological Processes*, *12*(10-11), 1537–1546. https://doi.org/10.1002/(SICI)1099-1085(199808/09)12:10/11<1537::AID-HYP679>3.0.CO;2-A

Romano, F., Cimini, D., Nilo, S. T., Di Paola, F., Ricciardelli, E., Ripepi, E., & Viggiano, M. (2017). The role of emissivity in the detection of arctic night clouds. *Remote Sensing*, *9*(5), 406. https://doi.org/10.3390/rs9050406

Schneider, P., Ghent, D., Corlett, G., Prata, F., & Remedios, J. (2012). Land surface temperature validation protocol (Report to European Space Agency) *Rep*.

Seemann, S. W., Borbas, E. E., Knuteson, R. O., Stephenson, G. R., & Huang, H.-L. (2008). Development of a global infrared land surface emissivity database for application to clear sky sounding retrievals from multispectral satellite radiance measurements. *Journal of Applied Meteorology and Climatology*, *47*(1), 108–123. https://doi.org/10.1175/2007JAMC1590.1

Serreze, M. C., & Barry, R. G. (2011). Processes and impacts of Arctic amplification: A research synthesis. *Global and Planetary Change*, *77*(1-2), 85–96. https://doi.org/10.1016/j.gloplacha.2011.03.004

Steinke, S., Eikenberg, S., Löhnert, U., Dick, G., Klocke, D., Di Girolamo, P., & Crewell, S. (2015). Assessment of small-scale integrated water vapour variability during HOPE. *Atmospheric Chemistry and Physics*, *15*(5), 2675–2692.

Tedesco, M., Box, J. E., Cappelen, J., Fausto, R. S., Fettweis, X., Hansen, K., et al. (2016). Greenland ice sheet *Rep*., NOAA Arctic Program.

Timmermans, M.-L. (2016). Sea surface temperature *Rep*., NOAA Arctic Program.

Van de Wal, R., Greuell, W., van den Broeke, M. R., Reijmer, C., & Oerlemans, J. (2005). Surface mass-balance observations and automatic weather station data along a transect near Kangerlussuaq, West Greenland. *Annals of Glaciology*, *42*(1), 311–316.

Van den Broeke, M., Smeets, C., & Van de Wal, R. (2011). The seasonal cycle and interannual variability of surface energy balance and melt in the ablation zone of the west Greenland ice sheet. *The Cryosphere*, *5*(2), 377–390. https://doi.org/10.5194/tc-5-377-2011

Veal, K. L., Corlett, G. K., Ghent, D., Llewellyn-Jones, D. T., & Remedios, J. J. (2013). A time series of mean global skin SST anomaly using data from ATSR-2 and AATSR. *Remote Sensing of Environment*, *135*, 64–76. https://doi.org/10.1016/j.rse.2013.03.028

Vihma, T., & Pirazzini, R. (2005). On the factors controlling the snow surface and 2-m air temperatures over the Arctic sea ice in winter. *Boundary-Layer Meteorology*, *117*(1), 73–90. https://doi.org/10.1007/s10546-004-5938-7

Vogelmann, H., Sussmann, R., Trickl, T., & Reichert, A. (2015). Spatiotemporal variability of water vapor investigated using lidar and FTIR vertical soundings above the Zugspitze. *Atmospheric Chemistry and Physics*, *15*(6), 3135–3148. https://doi.org/10.5194/acp-15-3135-2015

Wan, Z. (2014). New refinements and validation of the collection-6 MODIS land-surface temperature/emissivity product. *Remote Sensing of Environment*, *140*(140), 36–45. https://doi.org/10.1016/j.rse.2013.08.027

Woolway, R. I., Carrea, L., Merchant, C. J., Dokulil, M., de Eyto, E., DeGasperi, C., et al. (2017). Lake surface temperature [in "State of the Climate in 2016"]. *Bulletin of the American Meteorological Society*, *98*(8), 13–14.

Yan, B., Weng, F., & Meng, H. (2008). Retrieval of snow surface microwave emissivity from the advanced microwave sounding unit. *Journal of Geophysical Research*, *113*, D19206. https://doi.org/10.1029/2007JD009559

Zhong, X., Zhang, T., Kang, S., Wang, K., Zheng, L., Hu, Y., & Wang, H. (2018). Spatiotemporal variability of snow depth across the Eurasian continent from 1966 to 2012. *The Cryosphere*, *12*(1), 227–245. https://doi.org/10.5194/tc-12-227-2018